



Interactions of Transition Metal Dichalcogenide Nanosheets With Mucin: Quartz Crystal Microbalance With Dissipation, Surface Plasmon Resonance, and Spectroscopic Probing

Boshi Liu^{1,2,3}, Tao Yu², Renliang Huang^{1*}, Rongxin Su^{2,4*}, Wei Qi^{2,4} and Zhimin He²

¹ Tianjin Key Laboratory of Indoor Air Environmental Quality Control, School of Environmental Science and Engineering, Tianjin University, Tianjin, China, ² State Key Laboratory of Chemical Engineering, Tianjin Key Laboratory of Membrane Science and Desalination Technology, School of Chemical Engineering and Technology, Tianjin University, Tianjin, China, ³ School of Pharmaceutical Engineering of Traditional Chinese Medicine, Tianjin University of Traditional Chinese Medicine, Tianjin, China, ⁴ Collaborative Innovation Center of Chemical Science and Engineering (Tianjin), Tianjin, China

OPEN ACCESS

Edited by:

Jose Luis Sanchez,
University of Zaragoza, Spain

Reviewed by:

Jianxun Ding,
Changchun Institute of Applied
Chemistry (CAS), China
Shinji Takeoka,
Waseda University, Japan

*Correspondence:

Renliang Huang
tjuhl@tju.edu.cn
Rongxin Su
surx@tju.edu.cn

Specialty section:

This article was submitted to
Chemical Engineering,
a section of the journal
Frontiers in Chemistry

Received: 30 November 2018

Accepted: 05 March 2019

Published: 29 March 2019

Citation:

Liu B, Yu T, Huang R, Su R, Qi W and
He Z (2019) Interactions of Transition
Metal Dichalcogenide Nanosheets
With Mucin: Quartz Crystal
Microbalance With Dissipation,
Surface Plasmon Resonance, and
Spectroscopic Probing.
Front. Chem. 7:166.
doi: 10.3389/fchem.2019.00166

Ultrathin 2-dimensional transition metal dichalcogenides (TMDs) have become a class of high-potential materials in biomedicine due to their intriguing properties. They have been applied to solve biomedical challenges, such as biosensing, bioimaging, drug delivery, and cancer therapy. However, studies of the interactions between these materials and biomolecules are insufficient. Mucous tissue serves as a barrier to foreign hazardous substances and a gel layer for substance exchange. The main organic matter of mucous tissue is mucin, so it was selected as a model biomolecule to study its interactions with six different TMD nanosheets (NSs), including single-layered (SL), few-layered (FL), and small few-layered (SFL) MoS₂ and WS₂ NSs, using quartz crystal microbalance (QCM) with a dissipation monitor (QCM-D) and surface plasmon resonance (SPR). Additionally, UV absorption, fluorescence, and circular dichroism (CD) spectroscopy were applied to investigate the mechanism of the interactions and to study the conformational change of mucin. We found that the TMD NSs could adsorb on the mucin layer and affect its viscoelasticity. The results indicated that the SL WS₂ NSs exhibited the highest initial absorption rate and the maximum absorption amount, while the SL MoS₂ NSs exhibited the highest initial desorption rate. During the adsorption, the viscoelasticity variations of the mucin layer caused by the WS₂ nanosheets were weaker than those caused by the MoS₂ nanosheets. Furthermore, the conformational changes of mucin caused by the SL MoS₂, SL WS₂, and SFL MoS₂ NSs were higher than those resulting from other TMD NSs. These findings provide important information on the interactions between TMD NSs and mucin and provide useful insights into the interfacial behavior of TMD NSs before they enter tissues.

Keywords: transition metal dichalcogenide nanosheets, mucin, interactions, quartz crystal microbalance, surface plasmon resonance

INTRODUCTION

Mucus is secreted by specialized goblet cells in the columnar epithelium and serves many functions including lubrication, maintenance of a hydrated layer over the epithelium, a barrier to hazardous substances, and a permeable gel layer for the exchange of gases and nutrients with the underlying cells and tissues (Bansil and Turner, 2006; Linden et al., 2008; McGuckin et al., 2011; Demouveau et al., 2018). The main organic component that is responsible for the functions is mucin, which is heavily glycosylated with complex oligosaccharides (Hollingsworth and Swanson, 2004; Bansil and Turner, 2006; Feiler et al., 2007; Pelaseyed et al., 2014). Therefore, mucin is closely related to many mucus-related diseases, the intake of nutrients, and the adsorption and delivery of drugs through the mucus barrier (Bansil and Turner, 2006; Boya et al., 2017).

Two-dimensional nanosheets of transition metal dichalcogenides (TMDs) are fundamentally and technologically intriguing (Chhowalla et al., 2013; Tan and Zhang, 2015); in particular, MoS₂ and WS₂ have attracted interest as they possess a band gap, which is important for integration into electronic device structures. TMDs have provided great opportunities to solve the challenging problems in biomedicine (Li et al., 2017; Zhang et al., 2018), including but not limited to biosensing (Song et al., 2014; Chen et al., 2017; Singhal et al., 2018), bioimaging (Cheng et al., 2014; Liu et al., 2015; Choi et al., 2017; Song et al., 2017), drug delivery (Liu et al., 2014; Yin et al., 2014; Chen et al., 2017; Dong et al., 2018), and cancer therapy (Cheng et al., 2014; Liu et al., 2015; Qian et al., 2015; Song et al., 2017). However, TMDs could potentially be risky to human health and the environment (Guiney et al., 2015, 2018; Kumar et al., 2017). For example, MoS₂ has been shown to be toxic toward planktonic cells, biofilms, and mammalian cells in the presence of electron donors (Fan et al., 2015), to bind to the K⁺ channels and disturb their functions (Gu et al., 2018), to activate TGF-beta/Smad pathways and perturb the metabolome of human dermal fibroblasts (Yu et al., 2017), and to exhibit cytotoxicity and impact inflammation (Moore et al., 2017).

Sufficient assessments of the hazards of 2D TMD nanosheets (TMD NSs) should be conducted before the biomedical applications of such novel inorganic nanomaterials. However, there are only a few studies on the interaction between TMD NSs and proteins via molecular simulation (Fan et al., 2017; Xiao et al., 2018). Therefore, in this work, we conducted experimental studies on the interactions between TMD NSs and mucin. As mucin achieves its physiological functions in mucosal tissue as a supported hydrogel layer on the epithelial cells, we coated this glycoprotein onto the gold sensing chip of quartz crystal microbalance (QCM) and surface plasmon resonance (SPR) apparatus to form a hydrogel layer and mimic the mucosa and to investigate its interactions with TMD NSs during the adsorption and desorption. Spectroscopic methods, including UV absorbance spectroscopy, fluorescence quenching spectroscopy, and circular dichroism (CD) spectroscopy were also applied to further verify the results obtained from the QCM and SPR study, investigate the mechanism of the

interactions, and study the conformational change of mucin during the interactions.

MATERIALS AND METHODS

Materials

Mucin from bovine submaxillary gland was purchased from Shanghai Yuanye Biotech Co., Ltd, China. TMD NS aqueous dispersions (0.1 mg/mL) were purchased from XFANO Materials Tech Co., Ltd, and the layered NSs were prepared via the lithium intercalating method. The product information of these TMD NS aqueous dispersions was provided by the supplier and listed in **Table 1**. The thickness was obtained by AFM and single layer percentage was obtained by TEM. All of the data were acquired via statistics of the results from multiple experiments. All solutions were prepared using ultrapure water (18.2 MΩ·cm⁻¹, Sartorius Arium Pro VF, Germany).

Measurement of Size and Electrophoretic Mobility of the TMD NSs

The TMD NS aqueous dispersions were diluted to 0.01 mg/mL with ultrapure water. Thereafter, the hydrodynamic diameter and the electrophoretic mobility (EPM) of the TMD NSs was measured using a zetasizer (Malvern Nano ZS, UK).

QCM Study

QCM (Q-Sense E1, Biolin, Sweden) was applied to monitor the real-time mass and viscoelasticity change of the mucin layer during its interaction with the TMD NSs. Prior to the experiments, the bare gold chips were cleaned following the protocol in the QCM with a dissipation monitor (QCM-D) manual. Briefly, the gold chips were treated in a UV-ozone cleaner (PSD-UV8, Novascan, USA) for 30 min to destroy the organic matters and then soaked in 75% ethanol and cleaned in an ultrasonic cleaner for 30 min, followed by thorough rinsing with ultrapure water and drying with nitrogen. During the QCM experiments, the flow rate was set as 60 μL/min maintaining a laminar flow in the sensing module. Ultrapure water flowed through the channel at the beginning of each experiment, and after the signal of frequency (*F*) and dissipation (*D*) became stable, samples were added following the stages below. (I) The formation of mucin: 0.2 mg/mL mucin aqueous solution flowed over for ~20 min and coated the bare gold chip, forming a layer of mucin on its surface. (II) The rinsing of the mucin layer: ultrapure water was flowed over the mucin for ~10 min to remove the unstably combined mucin. (III) The interaction of TMD NS and the mucin layer: a 0.1 mg/mL TMD NS dispersion was flowed through the channel for ~45 min, giving a sufficient interaction with the mucin layer. (IV) Desorption: ultrapure water was flowed into the channel again. The signal of *F* and *D* at the seventh overtone of each experiment was recorded for the study.

SPR Study

An SPR apparatus (SPR Navi 200, BioNavis, Finland) was used to real-time monitor the refractive index of the materials during the interactions between the TMD NSs and mucin layer. The bare

TABLE 1 | Sample information of TMD NS aqueous dispersions.

Sample	Single-layered MoS ₂	Single-layered WS ₂	Few-layered MoS ₂	Few-layered WS ₂	Small few-layered MoS ₂	Small few-layered WS ₂
Abbreviation	SL MoS ₂	SL WS ₂	FL MoS ₂	FL WS ₂	SFL MoS ₂	SFL WS ₂
Thickness (nm)	~1	~1	1–10	1–10	1–10	1–10
Single layer percentage (%)	≥90	≥90	1–10	1–10	1–10	1–10

gold SPR chips were cleaned using the method mentioned in the “2.3. QCM study” session. At the beginning of each experiment, the twelve-way valve was set to “Load,” and the 100 μ L sample loops were filled with a 0.2 mg/mL mucin aqueous solution. Ultrapure water flowed as a running buffer at the rate of 5 μ L/min to maintain a laminar flow. After the stable signal of the SPR angle was achieved, the 12-way valve was set to “Inject,” and the mucin solution flowed over the bare gold chip and formed a mucin layer on its surface. The twelve-way valve was set to “Load” again after the mucin solution was exhausted, and the sample loops were filled with 0.1 mg/mL TMD NS dispersions. Then, the flow rate was set to 2 μ L/min, and the twelve-way valve was set to “Inject,” resulting in a slow flow of the TMD NS dispersions over the mucin and a sufficient interaction with it. The experiment was terminated after the TMD NS dispersions in the sample loops were exhausted.

The Spectroscopy Studies

UV absorption spectra, fluorescence spectra and CD spectra were applied to investigate the interactions between the TMD NSs and mucin in the aqueous phase. TMD NS dispersions and mucin aqueous solutions were fully mixed and interacted for 2 min at room temperature, and then the spectroscopy spectra of the mixtures were measured. In the UV and fluorescence spectroscopy experiments, the final concentration of mucin was 0.1 mg/mL, while in the CD measurement, it was 0.5 mg/mL. The UV absorption measurements were performed using a TU-1810 spectrophotometer (Persee, China), and the fluorescence spectra were evaluated using a Cary Eclipse fluorescence spectrometer (Varian, USA). A J-810 CD spectrometer (Jasco, Japan) was used for CD spectrum determinations. The TMD dispersions with the same concentration as in the mixtures were used as a reference sample in all of the spectroscopy measurements.

RESULTS AND DISCUSSION

Size and Electrophoretic Mobility of the TMD NSs

The interactions between proteins and nanomaterials are related to the physicochemical properties of the nanomaterials, including size and surface charge (Xia et al., 2015; Sun et al., 2018). Hydrodynamic diameter is the diameter of an imaginary sphere, which has the same diffusion rate as the real particle (Lattuada et al., 2003). The hydrodynamic diameters of the TMD NSs were measured by the Nano ZS Zetasizer based on the principle of dynamic light scattering and the Brownian movement of the sample, and the results were achieved through

the calculation by the software through the Stokes-Einstein equation. The hydrodynamic diameters of the TMD NSs were compared in **Figure 1A**. There was no significant difference in the hydrodynamic diameters of the single-layered and few-layered TMD NSs, although the single layer percentage was different. The hydrodynamic diameters of the small few-layered (SFL) TMD NSs were smaller than others. The TEM pictures of MoS₂ nanosheets were shown in **Supplementary Figure 1** for reference. A sketch (**Supplementary Figure 2**) was given according to the product information of the TMD NSs, and the results mentioned above to show the morphology of the TMD NSs. Among all the TMD NSs in this study, SL MoS₂ and SL WS₂ had the biggest diameters and the smallest thicknesses, while SFL MoS₂ and SFL WS₂ were smallest in diameter and biggest in thickness. FL MoS₂ and FL WS₂ were in the middle. Herein, “flakiness” is noted to describe “the ratio of diameter and thickness,” so the single-layered TMD NSs were the highest in flakiness, while the SFL TMD NSs were the lowest.

The EPM values of the TMD NSs were compared in **Figure 1B**. All the TMD NSs exhibited negative charged surfaces and the EPM values of the TMD NSs were very close, indicating the similar mobility under the same electric field.

The Interactions Between the TMD NSs and Mucin Layer

Mucin usually covers the surface of the epithelial cells of the organisms forming a hydrogel layer (Li et al., 2013; Brandão et al., 2017), which constitutes the main part of the mucosal structure. A mucin layer, which mimicked the mucosa, was acquired on the surface of QCM- and SPR-sensing modules via flowing mucin aqueous solutions over the gold chips. Then, the changes of mass, viscoelasticity, and refractive index were evaluated during the interactions of TMD NS dispersions with the mucin layer.

Mass and Viscoelasticity Variation Studied by QCM

The principle of QCM is based on a piezoelectric effect (Reviakine et al., 2011). The variations of the resonant frequency (F) in odd overtones are measured to directly reflect the mass change of the materials on the surface of its sensing module via Sauerbrey equation (Mushi et al., 2014).

$$\Delta m = -C\Delta F \quad (1)$$

Where m is the mass, C is the sensitivity constant of the quartz crystal (17.7 ng cm²/Hz for this study). The attenuation of oscillation amplitudes at a certain overtone is described as

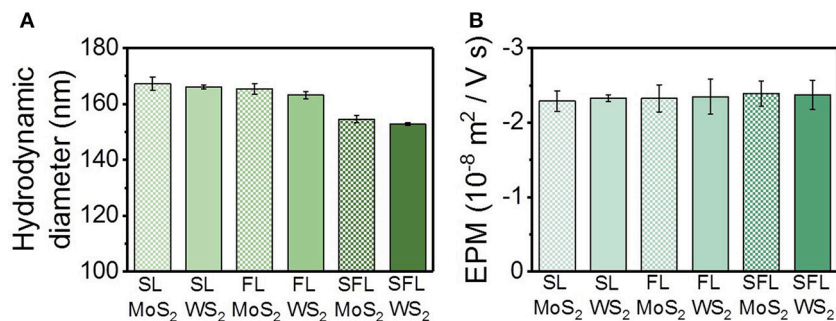


FIGURE 1 | Hydrodynamic diameter (A) and electrophoresis mobility (B) of the TMD NSs.

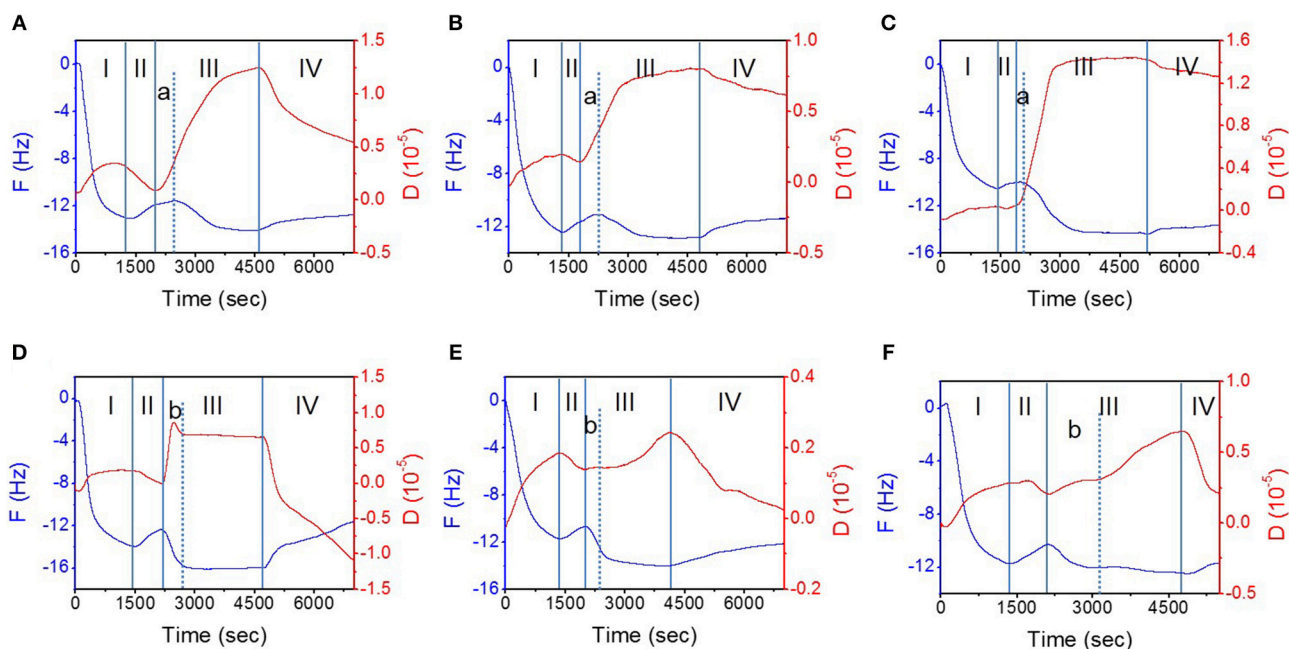
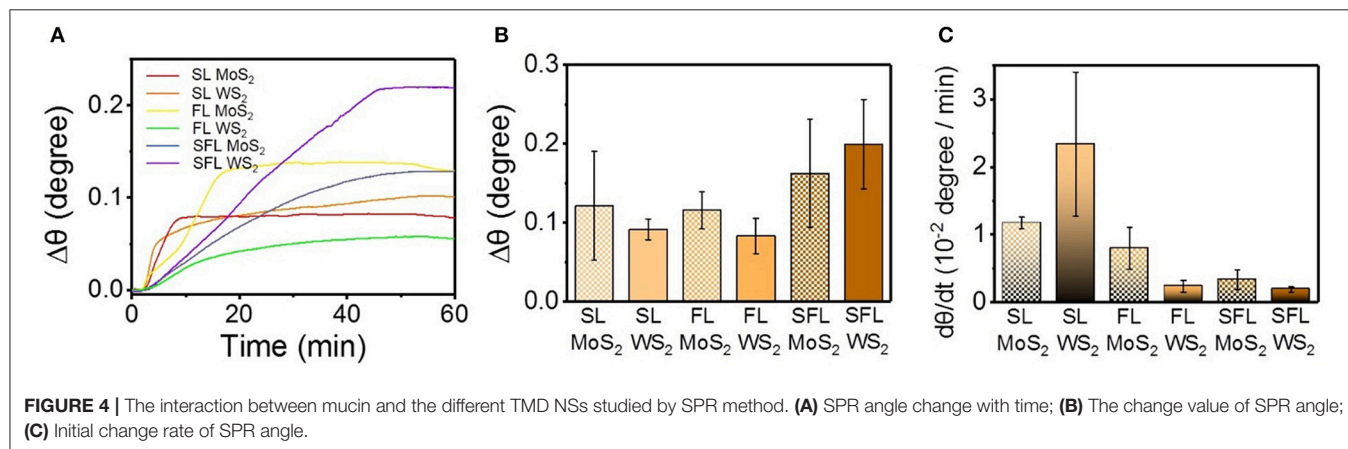
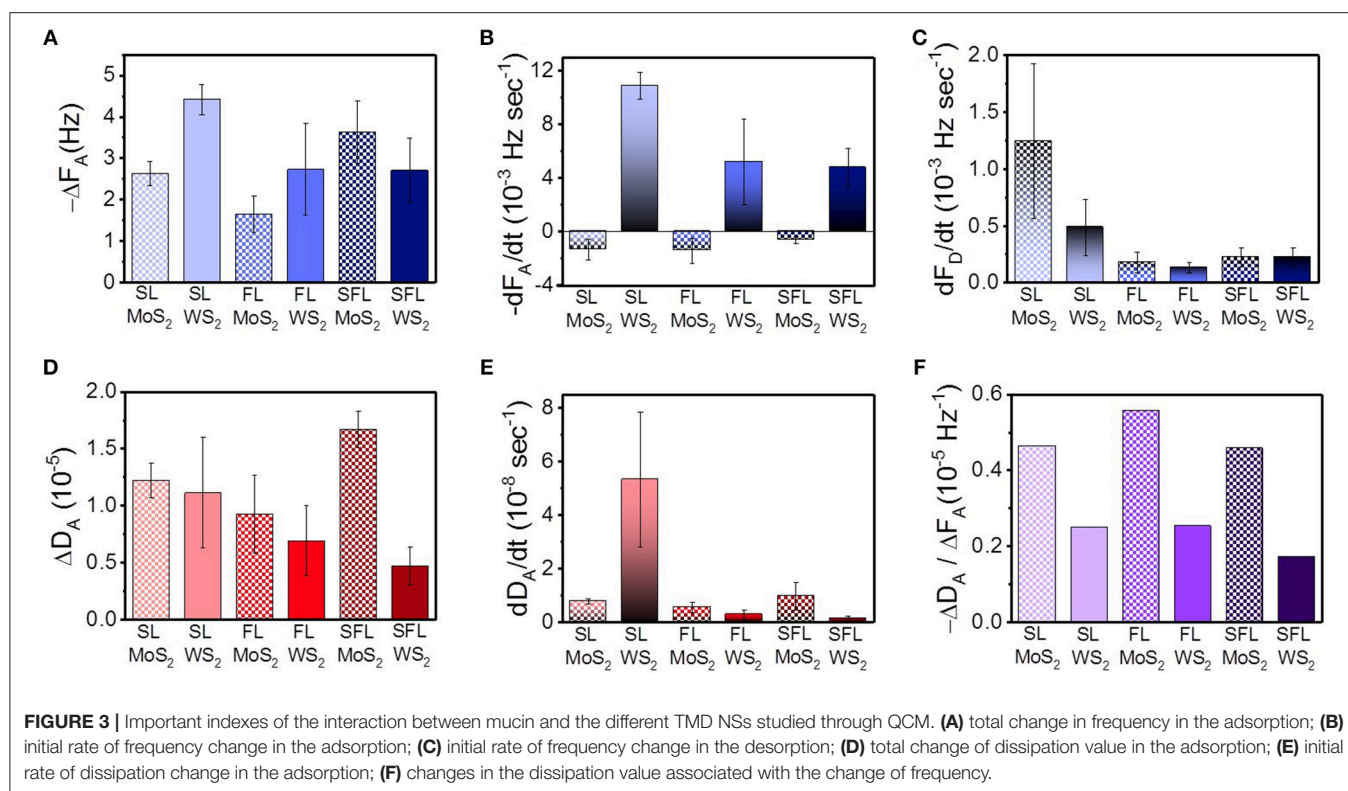


FIGURE 2 | The interaction of mucin hydrogel and TMD NSs studied by QCM. (A–F) Depict typical variation of the F and D values with time during the interaction of mucin and SL MoS₂, FL MoS₂, SFL MoS₂, SL WS₂, FL WS₂, and SFL WS₂, respectively. The stages (I–IV) are introduced in “2.3. QCM study” of the “Materials and Methods” section.

the dissipation (D), which gives information on the surface viscoelasticity (Yousefi and Tufenkji, 2016).

Figure 2 shows the variations of F and D values over time when the interaction between the different TMD NSs and the mucin layer occurred on the surface of the gold film chip. In the different experimental stages (described in section QCM Study), the trend of F and D variation is the same. In stage I, when the mucin aqueous solution flowed over the gold chip surface, the F value descended while the D value ascended owing to the increase of the mass and viscoelasticity of the materials on the surface, which indicated the adsorption of mucin on the surface of the QCM sensing module and the formation of a mucin layer. In stage II, ultrapure water was introduced to remove the unstably combined mucin. The F value ascended as the D value descended because of the slight desorption of mucin from the

gold surface. The average weight of the mucin layer formed on the sensing module was 197.7 ng/cm². In stage III, the F value decreased and the D value increased when TMD NS dispersions were flowed over the mucin layer, indicating an increased mass and viscoelasticity. In stage IV, an increase of the F value and a decrease of the D value were observed because of the desorption of the mucin and TMD NSs, which demonstrated a decrease of the mass and viscoelasticity. The main difference existed in stage III. When the MoS₂ NS dispersions flowed over the mucin layer (**Figures 2A–C**), slight increases of the F values were recorded at the beginning (shown as “stage a”), and the D values continued to increase. During “stage a,” the adsorption and desorption of the MoS₂ NSs, as well as the desorption of the mucin, occurred simultaneously, but the desorption rate of the MoS₂ NSs and mucin was higher than the adsorption rate of the MoS₂ NSs.



The duration of the “stage a” change trend was SL MoS₂ > FL MoS₂ > SFL MoS₂, indicating that the MoS₂ NSs with higher flakiness had a smaller initial adsorption rate, and they were more prone to cause the desorption of the mucin. On the other hand, a “stage b” was divided at the beginning inside the stage III. When FL WS₂ and SFL WS₂ interacted with mucin (**Figures 2E,F**), the *D* value rose slowly in “stage b,” and then the rate of rising increased. At the same time, the *F* value declined in “stage b,” and then the rate of decline decreased. These results revealed that in “stage b,” FL WS₂ and SFL WS₂ experienced fast adsorption to the mucin but did not severely enhance its viscoelasticity. Inversely, in “stage b,” the *F* value declined quickly, while the *D* value of SL WS₂ exhibited a very sharp increase followed by a

slight decline, indicating that SL WS₂ could quickly adsorb on mucin and severely affect its viscoelasticity.

Figure 3 was plotted in order to clearly compare the indexes of the interaction between the TMD NSs and mucin. In **Figure 3A**, $-\Delta F_A$ is the total change in frequency in the adsorption stage, which was the negative value of the minimum *F* value minus the *F* value at its beginning. It can reflect the maximum variation of mass during the whole adsorption stage. The mass variation of SL WS₂ was the highest among all of the TMD NSs, while the FL MoS₂ was the lowest. $-dF_A/dt$ in **Figure 3B** is the initial rate of frequency change in the adsorption stage, which was defined as a variation of the *F* value in the first 150 s of the adsorption stage, revealing the rate of mass change

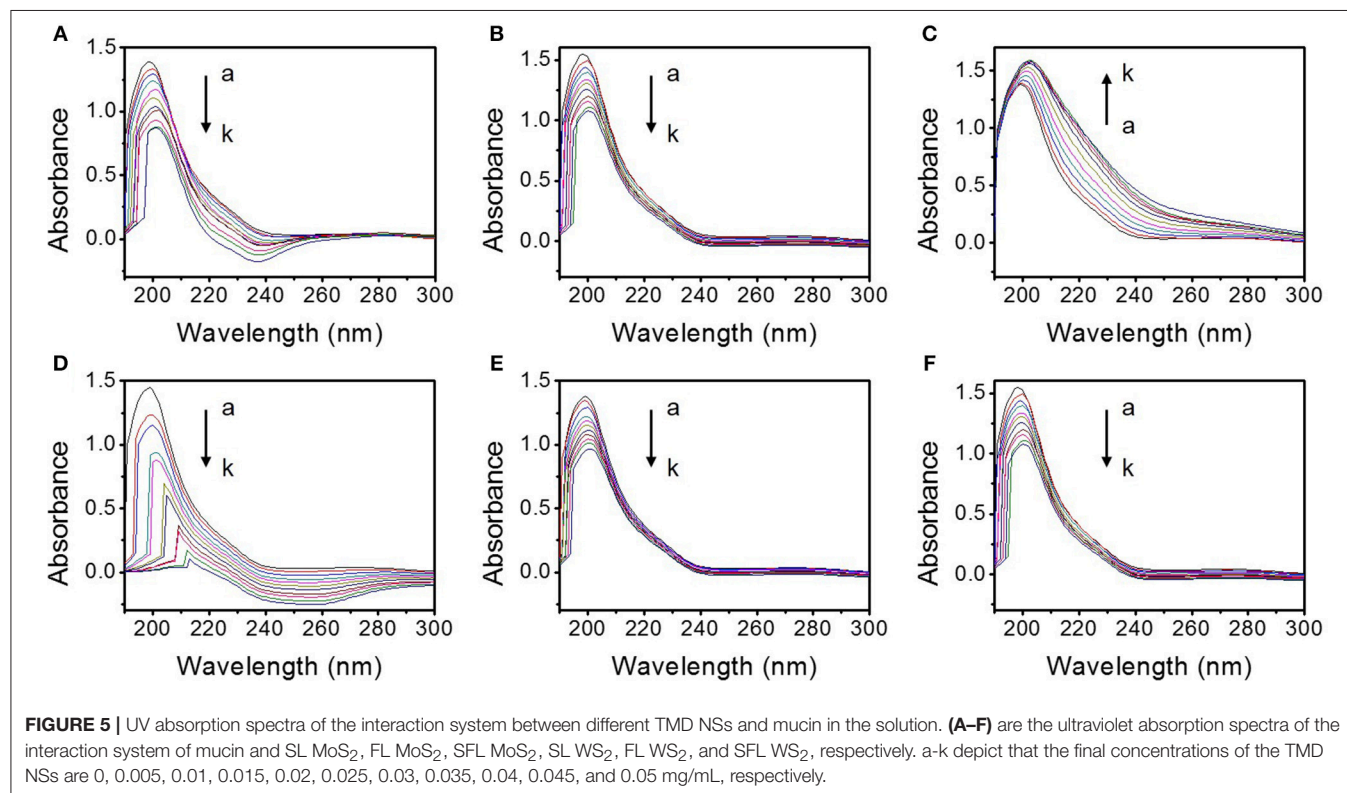
at the initial stage of adsorption. The $-dA/dt$ values of the WS₂ NSs were positive, among which the value of SL WS₂ was the highest, while the $-dF_A/dt$ values of the MoS₂ NSs were negative. Similarly, in **Figure 3C**, $-dF_D/dt$ is the initial rate of frequency change in the desorption stage, defined as the variation of F value in the first 150 s of the desorption stage, reflecting the rate of mass change at the initial stage of desorption. SL MoS₂ had the highest $-dF_D/dt$ value, while FL WS₂ had the lowest. In short, the results indicated that SL WS₂ exhibited the highest initial absorption rate and the maximum absorption amount, while the MoS₂ NSs had a negative initial adsorption rate, suggesting the desorption of mucin with MoS₂ at the beginning (stage a, as mentioned before). Additionally, the SL MoS₂ exhibited the highest initial desorption rate.

The viscoelasticity changes of the protein hydrogel layer can be caused by the changes in the structure of protein (Wang et al., 2010). In **Figure 3D**, we defined ΔD_A as the total change in dissipation in the adsorption stage, i.e., the maximum D in the adsorption stage minus the D value at its beginning. This index reveals the influence of the TMD NSs on the structure of the mucin in the whole adsorption stage. SFL MoS₂ was highest in this index, while SFL WS₂ was the lowest. In **Figure 3E**, dD_A/dt is the initial rate of dissipation change in the adsorption stage, which was defined as a variation of D value in the first 150 s of the adsorption stage. This index reflects the rate of viscoelasticity change and further reveals the intensity of the influence of the TMD NSs on the mucin structure at the initial stage of adsorption. The dD_A/dt value of SL WS₂ was much higher than

that of the other TMD NSs, indicating that it could rapidly affect the structure of mucin. In **Figure 3F**, $-\Delta D_A/\Delta F_A$ is the variation of the dissipation value accompanying the change in unit frequency in the adsorption stage, which gives information about the viscoelasticity change caused by per unit mass change. The $-\Delta D_A/\Delta F_A$ value of FL MoS₂ had the highest of all the TMD NSs, while the SFL WS₂ had the lowest $-\Delta D_A/\Delta F_A$ value. In general, the $-\Delta D_A/\Delta F_A$ value of the WS₂ NSs was smaller than that of the MoS₂ NSs, indicating that when the TMD NSs in the same mass adsorbed onto the mucin, the WS₂ NSs caused less influence on its viscoelasticity than the MoS₂ NSs. Based on the above experimental results, suitable TMD NSs can be selected for specific biomedical applications as demanded.

Refractive Index Studied by SPR

The refractive index of materials on the surface of the sensing chip can be detected in real-time via SPR study (Homola, 2008; Liu et al., 2016), and the variation of the refractive index of the protein layer is closely related with the conformational changes of the protein (Dell'Orco and Koch, 2016). **Figure 4A** shows the variation of the SPR angle (θ) with time, and $\Delta\theta$ is the difference between the SPR angle at a certain time and the initial SPR angle. It can be found that SL MoS₂, and FL MoS₂ tended to achieve a quick saturation within 20 min, while the other four kinds of TMD NSs tended to achieve a slower saturation over 40 min. $\Delta\theta$ in **Figure 4B** is the total variation of θ during the adsorption as the maximum of θ minus the initial θ . $d\theta/dt$ that was introduced to exhibit the initial variation of θ (**Figure 4C**),



which is defined as the variation of θ in the first 150 s of the adsorption stage. The $d\theta/dt$ value of SL WS₂ was much higher than the other TMD NSs, and this result was consistent with the dF_A/dt value of the adsorption in the QCM study. The $d\theta/dt$ value of the NSs with the same chemical constituents exhibited a decreasing trend with the lowered flakiness. The TMD NSs with higher flakiness tended to have higher $\Delta\theta$ and lower $d\theta/dt$.

The Interactions in the Aqueous Phase Studied by Spectroscopic Methods

UV Absorption Spectra

The influences of the different TMD NSs on the UV absorption spectra of mucin are shown in **Figure 5**. With the addition of the TMD NSs, the variation of the absorption peak of peptide bonds (~200 nm) can be clearly observed. FL MoS₂, FL WS₂, and SFL WS₂ caused smaller change of the UV absorption spectra than the other three TMD NSs. An obvious change at 240 nm was observed in the SL MoS₂ and mucin interaction system. SL WS₂ severely weakened the absorption peak of peptide bonds and made it significantly redshift, while the absorption peak of peptide bonds was redshifted and enhanced by the SFL MoS₂. These experimental results indicated that the conformation of mucin was not significantly affected by FL MoS₂, FL WS₂ and SFL WS₂, and the microenvironment of peptide bonds of mucin were severely changed in the presence of SL MoS₂, SL WS₂, and SFL MoS₂. The experimental

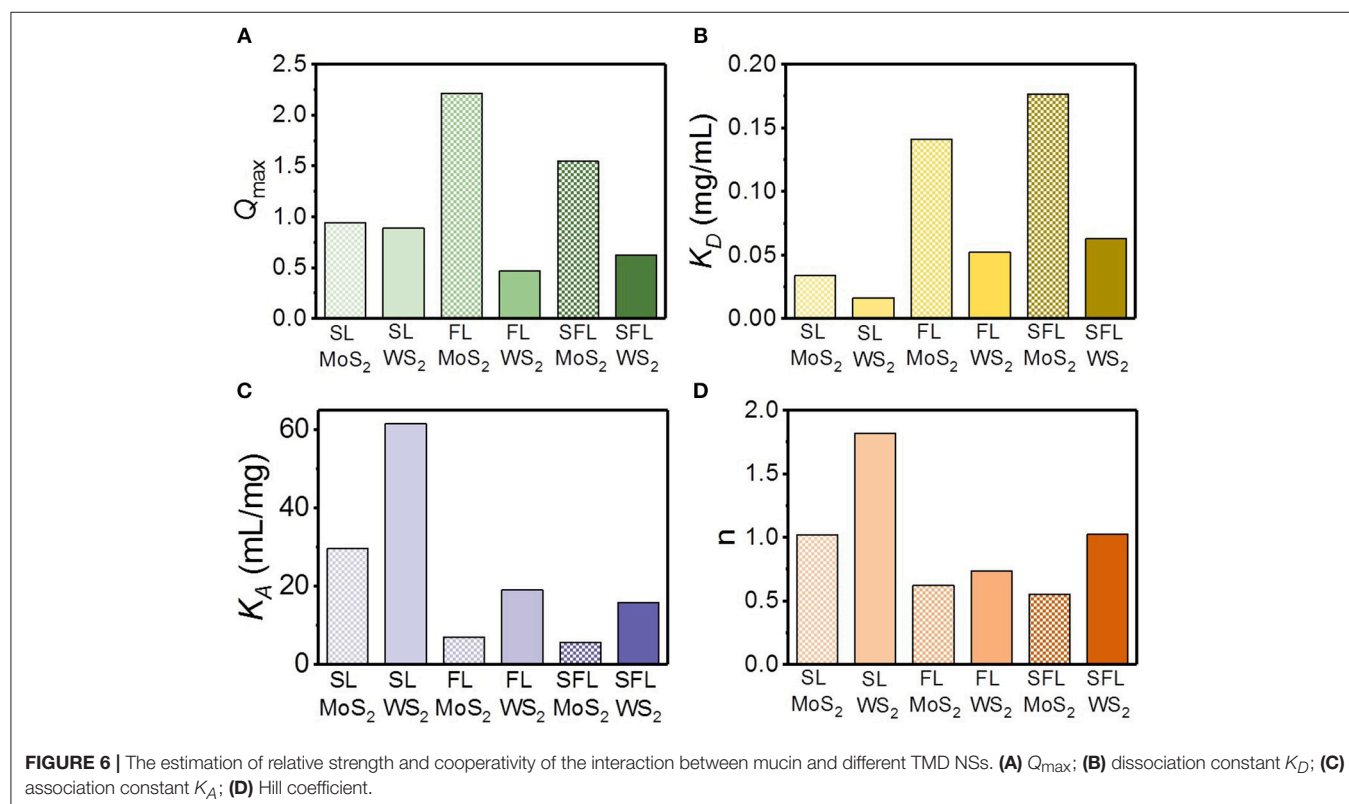
results are consistent with the dD_A/dt value in the “QCM study” section.

Fluorescence Quenching Spectra

The chromophore residues of proteins, including tryptophan, tyrosine and phenylalanine, can serve as intrinsic fluorescent probes, and these aromatic amino acid residues are sensitive to their microenvironment. Therefore, fluorescence quenching behaviors of mucin by the TMD NSs were characterized. As shown in **Supplementary Figure 3**, with the increase of the TMD NS concentration, the fluorescence of mucin was significantly quenched. The SL MoS₂, SL WS₂, and SFL MoS₂ exhibited higher quenching efficiency among the TMD NSs. This may result in stronger variation in the microenvironment of the chromophore residue of mucin, and possibly changes in its tertiary structure. The results are consistent with the change in UV-vis absorption spectra.

Shifts in the emission maximum wavelength of mucin with variations in the concentrations of the TMD NSs can be found in the normalized fluorescence spectra (**Supplementary Figure 4**). SL WS₂ caused the largest blueshift, followed by SFL MoS₂ and SL MoS₂. This kind of shift may demonstrate some changes in the microenvironment of the aromatic amino acid residues, as well as variations of the protein tertiary structure. The blueshifts indicate a decrease in the hydrophilicity of the emission-active residues of mucin (Zamolo et al., 2018).

Fluorescence quenching mechanisms include static quenching and dynamic quenching. Dynamic quenching refers to the



transfer of energy or electrons during the collision between the quenching agent and fluorescence active materials in the excited state, which does not affect the structure and activity of the protein. Static quenching refers to the quenching agent and fluorescence material interactions and generate a certain kind of ground-state complex without the emission of photons, and the fluorescence intensity is consequently reduced (Chi et al., 2010; Wang et al., 2011; Hao et al., 2017). Plots of fluorescence emission intensity I_0/I vs. the TMD NSs were given as **Supplementary Figure 5**, where I_0 and I represent the maximum fluorescence emission intensity of mucin in the absence and presence of the TMD NSs, respectively. When the final concentration of the TMD NSs was lower than 0.025 mg/mL, the fluorescence emission intensity exhibited a linear trend, which implies that the protein underwent a dynamic collisional quenching. With the higher concentration of the TMD NSs, the emission intensity of SL MoS₂, SL WS₂, FL MoS₂, and SFL MoS₂ exhibited an exponential trend, while that of FL WS₂ and SFL WS₂ maintained linearly. This reveals that when interacting with FL WS₂ and SFL WS₂, mucin kept dynamic quenching, but additional static quenching occurred when mucin interacted with SL MoS₂, FL MoS₂, SL WS₂, and SFL MoS₂. These results offer more evidence that SL MoS₂, FL MoS₂, SL WS₂, and SFL MoS₂ exerted a stronger influence on the conformation of mucin than FL WS₂ and SFL WS₂ did.

At low TMD NS concentrations, the fluorescence quenching was driven by diffusive transport, and the relative kinetic efficiency of the fluorescence quenching of mucin can be derived based on the non-equilibrium Stern-Volmer model (Kenry et al., 2016; Wani et al., 2018), as described in equation (1),

$$\frac{I_0}{I} = 1 + K_{SV}C_Q \quad (2)$$

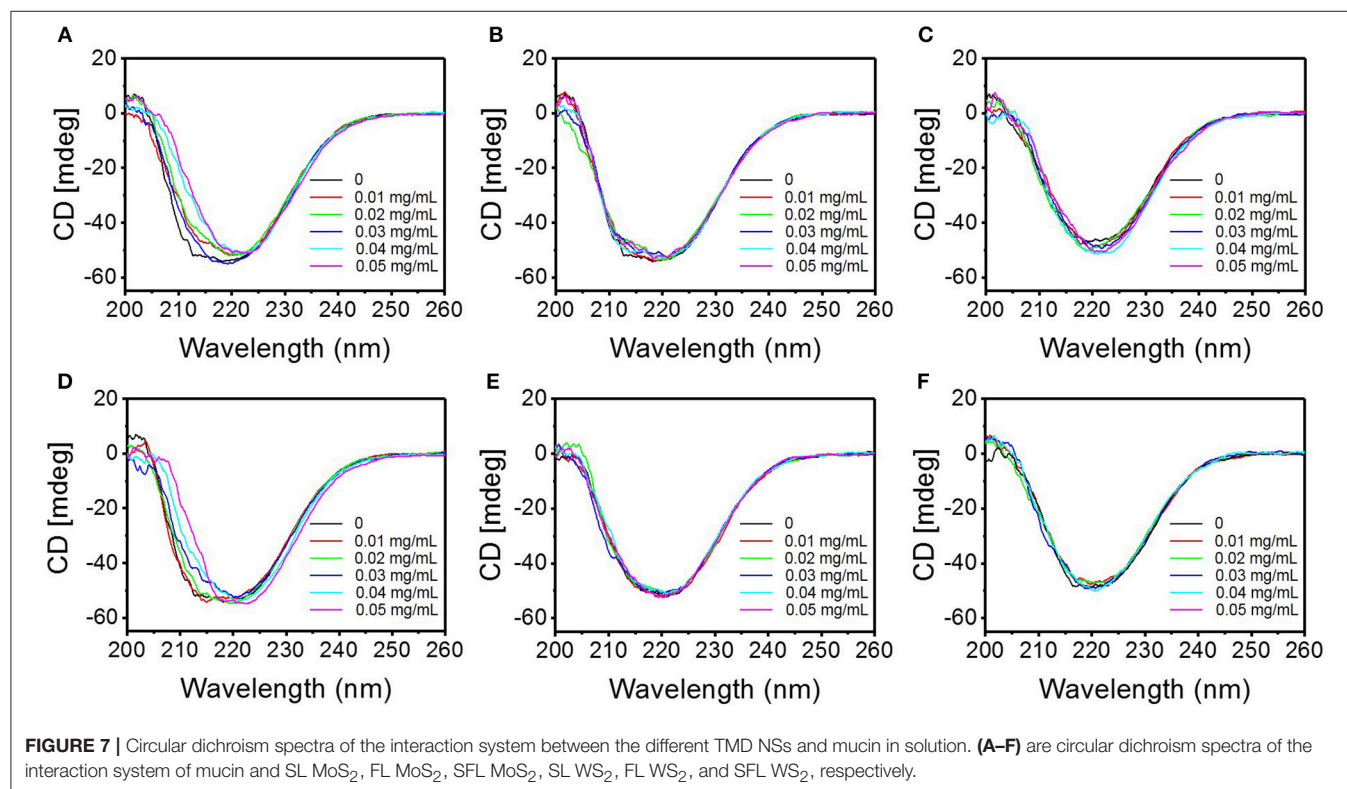
Where K_{SV} is the Stern-Volmer constant signifying the fluorescence quenching efficiency, and C_Q is the concentration of the quenching agent. The K_{SV} values are compared in **Supplementary Figure 6**. SL MoS₂ and SL WS₂ exhibited higher quenching efficiency than other TMD NSs. These two TMD NSs were the highest in flakiness, implying a higher relative surface area and resulting in a more efficient fluorescence quenching.

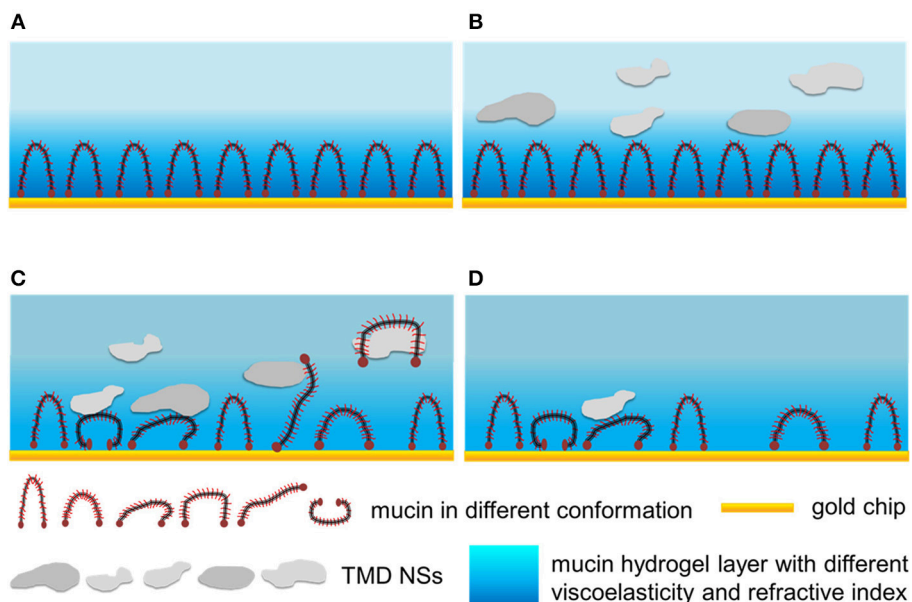
The relative strength and cooperativity of the interaction of the TMD NSs and mucin were further studied based on the quantification of several key parameters, including the binding dissociation constant K_D , binding association constant K_A (the reciprocal of K_D), and the Hill coefficient n . These parameters can be obtained through the Hill equations as follows:

$$Q = \frac{(I_0 - I)}{I_0} \quad (3)$$

$$\frac{Q}{Q_{\max}} = \frac{C_Q^n}{K_D^n + C_Q^n} \quad (4)$$

Where Q_{\max} is the saturation value of Q , which can be derived through non-linear fit of fluorescence quenching (**Figure 6A**; **Supplementary Figure 7**). K_D is the equilibrium binding dissociation constant, which describes the relative





SCHEME 1 | The interactions between TMD NSs and mucin in the mimic mucosa on the surface of QCM-D and SPR sensor chips. **(A)** The formation of mucin hydrogel layer. **(B)** TMD NSs adsorbed on the mucin layer. **(C)** TMD NSs interacted with the mucin layer, resulting in the conformational changes of mucin, and the formation of mucin-TMD NS complexes. **(D)** TMD NS-mucin complex fell off from the gold surfaces after thorough washing.

strength of the TMD NS–mucin interaction, and n is the Hill coefficient, which defines the cooperativity of the TMD NS–mucin association. As displayed in **Figures 6B,C**, the K_D value of the MoS₂ NSs was higher than that of the WS₂ NSs in the same hydrodynamic diameter. In addition, for the TMD NSs with the same element, the higher the flakiness was, the higher K_A value was. These results imply that the WS₂ NSs tend to be easier to associate with mucin than the MoS₂ NSs and that the NSs with higher relative surface area (the SL NSs) have a stronger association with mucin. The Hill coefficient n describes the binding cooperativity between the TMD NSs and mucin (**Figure 6D**). The SL WS₂-mucin complex exhibited cooperative binding with positive cooperativity ($n > 1$), implying that an increased amount of mucin adsorbed onto the surface of SL WS₂ will enhance the binding strength between the proteins and the surface. In contrast, the FL MoS₂-mucin, FL WS₂-mucin, and SFL MoS₂-mucin complexes displayed anti-cooperative binding with negative cooperativity ($n < 1$). This indicates that the more mucin that is adsorbed on the surface of these TMD NSs, the weaker binding strength will be.

CD Spectroscopy

CD spectroscopy is an effective tool for rapid determination of secondary structure of proteins (Greenfield, 2006). It is widely used to determine the fold of purified proteins and the influence on their conformation or stability caused by the microenvironment changes (Murtaza et al., 2018). Far ultraviolet CD spectra (200–260 nm), which reveal the variations in the secondary structure of the proteins resulted from the interaction between proteins and other substances (Kenry et al., 2017), were investigated to describe the interaction between the TMD NSs

and mucin (**Figure 7**). With the increasing of the concentration of TMD NSs, the CD spectra of the interaction systems between mucin and FL MoS₂, FL WS₂, and SFL WS₂ did not exhibit much variation, while SL MoS₂ and SL WS₂ caused the CD spectra of mucin to redshift, and SFL MoS₂ slightly enlarged the peak of CD spectra. These experiment results were in accordance with the trends of UV spectra variation as mentioned.

The analysis of secondary structure variation of mucin was conducted via CD Pro software. As shown in **Supplementary Figure 8**, sharp variation of the percentage of secondary structures in each typical sort did not occur when the final concentration of TMD NSs increased from 0.01 to 0.05 mg/mL. With the increasing of the concentration of TMD NSs, SFL MoS₂ increased the percentage of α -helix, and decreased the percentage of β -sheet. In contrast, the interaction of mucin with other TMD NSs made its percentage of α -helix higher, and β -sheet lower, and SL MoS₂ and SL WS₂ caused larger-scale variation. These results gave the information of conformational change of mucin during its interactions with the TMD NSs.

Mechanism of the Interactions Between the TMD NSs and Mucin

According to the results mentioned above, here a possible mechanism of the interactions between the TMD NSs and mucin was proposed, as shown in **Scheme 1**. When the mucin solution flowed over the gold chip, the protein adhered onto the gold surface and formed a hydrogel layer with water (**Scheme 1A**). When the dispersions of TMD NSs flowed over the mucin hydrogel layer, the mass, viscoelasticity and refractive index of the materials on the gold chip surface varied. These results

indicated that the TMD NSs adsorbed and interacted with the mucins, resulting in their conformational changes, and the variation of their amino acid residues' microenvironments (Schemes 1B,C). In this stage, SL WS₂ can quickly adsorb on the mucin layer, and the viscoelasticity variations of the mucin layer caused by the MoS₂ nanosheets were more intense than those caused by the WS₂ nanosheets. It was observed in the spectroscopic probing that SL MoS₂, SL WS₂, and SFL MoS₂ caused higher the conformational changes of mucin than the other three TMD NSs. TMD NSs interact with mucin molecules by hydrophobic effect. The TMD NS-mucin complex probably fell off from the gold surfaces after the thorough washing, thus resulting in the increased *F* value and the decreased *D* value (Scheme 1D). In this stage, SL MoS₂ exhibited the highest initial desorption rate.

Mucin consists of a protein core and glycosyls in its common structure. The protein core is arranged into distinct regions. The central glycosylated region is comprised of a large number of tandem repeats that are rich in serine, threonine and proline, while the regions with an amino acid composition more representative of globular proteins are located at the terminals. The central glycosylated region is highly glycosylated consisting of ~80% carbohydrates primarily *N*-acetylgalactosamine, *N*-acetylglucosamine, fucose, galactose, and sialic acid, and the glycosyls are arranged in a "bottle brush" configuration around the protein core (Bansil and Turner, 2006). The central glycosylated region is weakly negatively charged owing to the carboxyl groups. As the TMD NSs are also negatively charged, the adsorption of TMD NSs can be hindered by the electrostatic repulsion. On the other hand, the TMD NSs with a large surface energy were able to be adsorbed on the mucin layer via the non-covalent interaction, such as the van der Waals' force, hydrogen binding, and hydrophobic interaction, and some of the TMD NSs interacted with the mucin proteins, to form a NS-mucin complex. The NS-mucin complex and the large-sized TMD NSs desorbed from the sensor surfaces following the washing buffer step, thus resulting in an increased *F* value and a decreased *D* value (Figure 2).

REFERENCES

- Bansil, R., and Turner, B. S. (2006). Mucin structure, aggregation, physiological functions and biomedical applications. *Curr. Opin. Colloid Interface Sci.* 11, 164–170. doi: 10.1016/j.cocis.2005.11.001
- Boya, V. N., Lovett, R., Setua, S., Gandhi, V., Nagesh, P. K. B., Khan, S., et al. (2017). Probing mucin interaction behavior of magnetic nanoparticles. *J. Colloid Interface Sci.* 488, 258–268. doi: 10.1016/j.jcis.2016.10.090
- Brandão, E., Santos Silva, M., García-Estévez, I., Mateus, N., de Freitas, V., and Soares, S. (2017). Molecular study of mucin-procyanidin interaction by fluorescence quenching and Saturation Transfer Difference (STD)-NMR. *Food Chem.* 228, 427–434. doi: 10.1016/j.foodchem.2017.02.027
- Chen, S.-C., Lin, C.-Y., Cheng, T.-L., and Tseng, W.-L. (2017). Sensors: 6-Mercaptopurine-induced fluorescence quenching of Monolayer MoS₂ nanodots: applications to glutathione sensing, cellular imaging, and glutathione-stimulated drug delivery. *Adv. Funct. Mater.* 27:702452. doi: 10.1002/adfm.201702452

CONCLUSIONS

In summary, we demonstrated the interactions between mucin and TMD NSs using QCM-D, SPR, and spectroscopic methods, including UV absorption spectroscopy, fluorescence quenching spectroscopy, and CD spectroscopy. The results indicated that the TMD NSs adsorbed on the mucin layer and affected its viscoelasticity and refractive index. SL WS₂ exhibited the highest initial absorption rate and the maximum absorption amount, while SL MoS₂ exhibited the highest initial desorption rate. During the adsorption, the viscoelasticity variations of the mucin layer caused by the WS₂ nanosheets was weaker than that caused by the MoS₂ nanosheets. Furthermore, the conformational changes of mucin caused by SL MoS₂, SL WS₂, and SFL MoS₂ were higher than those from other TMD NSs. This work provides insights on the interactions between TMD NSs and mucin. Suitable TMD NSs can be selected for specific biomedical applications based on the findings in this study.

AUTHOR CONTRIBUTIONS

BL, RH, and RS designed research. BL and TY performed research. All the authors analyzed data and wrote the paper and read and approved the final manuscript.

FUNDING

This work was supported by the National Natural Science Foundation of China (21621004, 21777112, 21776212), Tianjin Municipal Science and Technology Bureau, China (16JCZDJC37900, 18YFHBZC00010, 18YFZCSF00590), and the Ministry of Education (grant No. NCET-11-0372).

SUPPLEMENTARY MATERIAL

The Supplementary Material for this article can be found online at: <https://www.frontiersin.org/articles/10.3389/fchem.2019.00166/full#supplementary-material>

- Cheng, L., Liu, J. J., Gu, X., Gong, H., Shi, X. Z., Liu, T., et al. (2014). PEGylated WS₂ nanosheets as a multifunctional theranostic agent for *in vivo* dual-modal CT/Photoacoustic Imaging guided photothermal therapy. *Adv. Mater.* 26, 1886–1893. doi: 10.1002/adma.201304497
- Chhowalla, M., Shin, H. S., Eda, G., Li, L. J., Loh, K. P., and Zhang, H. (2013). The chemistry of two-dimensional layered transition metal dichalcogenide nanosheets. *Nat. Chem.* 5, 263–275. doi: 10.1038/nchem.1589
- Chi, Z., Liu, R., and Zhang, H. (2010). Noncovalent interaction of oxytetracycline with the enzyme trypsin. *Biomacromolecules* 11, 2454–2459. doi: 10.1021/bm100633h
- Choi, C., Choi, M. K., Liu, S. Y., Kim, M. S., Park, O. K., Im, C., et al. (2017). Human eye-inspired soft optoelectronic device using high-density MoS₂-graphene curved image sensor array. *Nat. Commun.* 8:1664. doi: 10.1038/s41467-017-01824-6
- Dell'Orco, D., and Koch, K. W. (2016). Fingerprints of calcium-binding protein conformational dynamics monitored by surface plasmon resonance. *ACS Chem. Biol.* 11, 2390–2397. doi: 10.1021/acscchembio.6b00470

- Demouveau, B., Gouyer, V., Gottrand, F., Narita, T., and Desseyn, J. L. (2018). Gel-forming mucin interactome drives mucus viscoelasticity. *Adv. Colloid Interface Sci.* 252, 69–82. doi: 10.1016/j.cis.2017.12.005
- Dong, X., Yin, W., Zhang, X., Zhu, S., He, X., Yu, J., et al. (2018). Intelligent MoS₂ nanotheranostic for targeted and enzyme-/pH-/NIR-responsive drug delivery to overcome cancer chemotherapy resistance guided by PET imaging. *ACS Appl. Mater. Interfaces* 10, 4271–4284. doi: 10.1021/acsami.7b17506
- Fan, H., Zhao, D., Li, Y., and Zhou, J. (2017). Lysozyme orientation and conformation on MoS₂ surface: insights from molecular simulations. *Biointerphases* 12:02D416. doi: 10.1116/1.4984803
- Fan, J. J., Li, Y. F., Nguyen, H. N., Yao, Y., and Rodrigues, D. F. (2015). Toxicity of exfoliated-MoS₂ and annealed exfoliated-MoS₂ towards planktonic cells, biofilms, and mammalian cells in the presence of electron donor. *Environ. Sci. Nano* 2, 370–379. doi: 10.1039/c5en00031a
- Feiler, A. A., Sahlholm, A., Sandberg, T., and Caldwell, K. D. (2007). Adsorption and viscoelastic properties of fractionated mucin (BSM) and bovine serum albumin (BSA) studied with quartz crystal microbalance (QCM-D). *J. Colloid Interface Sci.* 315, 475–481. doi: 10.1016/j.jcis.2007.07.029
- Greenfield, N. J. (2006). Using circular dichroism spectra to estimate protein secondary structure. *Nat. Protoc.* 1, 2876–2890. doi: 10.1038/nprot.2006.202
- Gu, Z., Plant, L. D., Meng, X. Y., Perez-Aguilar, J. M., Wang, Z. G., Dong, M. D., et al. (2018). Exploring the nanotoxicology of MoS₂: a study on the interaction of MoS₂ nanoflakes and K⁺ channels. *ACS Nano* 12, 705–717. doi: 10.1021/acsnano.7b07871
- Guiney, L., Mansukhani, N., Kim, P., Wang, X., Ji, Z. X., Chang, C. H., et al. (2015). “Toxicological potential and environmental fate of molybdenum disulfide (MoS₂), a post-graphene 2D material,” in *Abstracts of Papers of the American Chemical Society*. (Washington, DC), p. 250.
- Guiney, L. M., Wang, X., Xia, T., Nel, A. E., and Hersam, M. C. (2018). Assessing and mitigating the hazard potential of two-dimensional materials. *ACS Nano* 12, 6360–6377. doi: 10.1021/acsnano.8b02491
- Hao, C., Xu, G., Feng, Y., Lu, L., Sun, W., and Sun, R. (2017). Fluorescence quenching study on the interaction of ferrocene oxide nanoparticles with bovine serum albumin. *Spectrochim. Acta Part A Mol. Biomol. Spectrosc.* 184, 191–197. doi: 10.1016/j.saa.2017.05.004
- Hollingsworth, M. A., and Swanson, B. J. (2004). Mucins in cancer: protection and control of the cell surface. *Nat. Rev. Cancer* 4, 45–60. doi: 10.1038/nrc1251
- Homola, J. (2008). Surface plasmon resonance sensors for detection of chemical and biological species. *Chem. Rev.* 108, 462–493. doi: 10.1021/cr068107d
- Kenry, Geldert, A., Liu, Y. P., Loh, K. P., and Lim, C.T. (2017). Nanobio interactions between carbon nanomaterials and blood plasma proteins: why oxygen functionality matters. *Npg Asia Materials* 9:e422. doi: 10.1038/am.2017.129
- Kenry, Loh, K. P., and Lim, C.T. (2016). Molecular interactions of graphene oxide with human blood plasma proteins. *Nanoscale* 8, 9425–9441. doi: 10.1039/c6nr01697a
- Kumar, N., George, B. P. A., Abrahamse, H., Parashar, V., and Ngila, J. C. (2017). Sustainable one-step synthesis of hierarchical microspheres of PEGylated MoS₂ nanosheets and MoO₃ nanorods: their cytotoxicity towards lung and breast cancer cells. *Appl. Surf. Sci.* 396, 8–18. doi: 10.1016/j.apsusc.2016.11.027
- Lattuada, M., Wu, H., and Morbidelli, M. (2003). Hydrodynamic radius of fractal clusters. *J. Colloid Interface Sci.* 268, 96–105. doi: 10.1016/j.jcis.2003.07.028
- Li, L. D., Crouzier, T., Sarkar, A., Dunphy, L., Han, J., and Ribbeck, K. (2013). Spatial configuration and composition of charge modulates transport into a mucin hydrogel barrier. *Biophys. J.* 105, 1357–1365. doi: 10.1016/j.bpj.2013.07.050
- Li, X., Shan, J. Y., Zhang, W. Z., Su, S., Yuwen, L. H., and Wang, L. H. (2017). Recent advances in synthesis and biomedical applications of two-dimensional transition metal dichalcogenide nanosheets. *Small* 13:602660. doi: 10.1002/sml.201602660
- Linden, S. K., Sutton, P., Karlsson, N. G., Korolik, V., and McGuckin, M. A. (2008). Mucins in the mucosal barrier to infection. *Mucosal Immunol.* 1, 183–197. doi: 10.1038/mi.2008.5
- Liu, B. S., Liu, X., Shi, S., Huang, R. L., Su, R. X., Qi, W., et al. (2016). Design and mechanisms of antifouling materials for surface plasmon resonance sensors. *Acta Biomater.* 40, 100–118. doi: 10.1016/j.actbio.2016.02.035
- Liu, T., Shi, S. X., Liang, C., Shen, S. D., Cheng, L., Wang, C., et al. (2015). Iron oxide decorated MoS₂ nanosheets with double PEGylation for chelator-free radio labeling and multimodal imaging guided photothermal therapy. *ACS Nano* 9, 950–960. doi: 10.1021/nn506757x
- Liu, T., Wang, C., Gu, X., Gong, H., Cheng, L., Shi, X. Z., et al. (2014). Drug delivery with PEGylated MoS₂ nano-sheets for combined photothermal and chemotherapy of cancer. *Adv. Mater.* 26, 3433–3440. doi: 10.1002/adma.201305256
- McGuckin, M. A., Linden, S. K., Sutton, P., and Florin, T. H. (2011). Mucin dynamics and enteric pathogens. *Nat. Rev. Microbiol.* 9, 265–278. doi: 10.1038/nrmicro2538
- Moore, C., Movia, D., Smith, R. J., Hanlon, D., Lebre, F., Lavelle, E. C., et al. (2017). Industrial grade 2D molybdenum disulfide (MoS₂): an *in vitro* exploration of the impact on cellular uptake, cytotoxicity, and inflammation. *2D Mater.* 4:13. doi: 10.1088/2053-1583/aa673f
- Murtaza, A., Muhammad, Z., Iqbal, A., Ramzan, R., Liu, Y., Pan, S. Y., et al. (2018). Aggregation and conformational changes in native and thermally treated polyphenol oxidase from apple juice (*Malus domestica*). *Front. Chem.* 6:203. doi: 10.3389/fchem.2018.00203
- Mushi, N. E., Utsel, S., and Berglund, L. A. (2014). Nanostructured biocomposite films of high toughness based on native chitin nanofibers and chitosan. *Front. Chem.* 2:99. doi: 10.3389/fchem.2014.00099
- Pelasey, T., Bergstrom, J. H., Gustafsson, J. K., Ermund, A., Birchenough, G. M. H., Schutte, A., et al. (2014). The mucus and mucins of the goblet cells and enterocytes provide the first defense line of the gastrointestinal tract and interact with the immune system. *Immunol. Rev.* 260, 8–20. doi: 10.1111/imr.12182
- Qian, X. X., Shen, S. D., Liu, T., Cheng, L., and Liu, Z. (2015). Two-dimensional TiS₂ nanosheets for *in vivo* photoacoustic imaging and photothermal cancer therapy. *Nanoscale* 7, 6380–6387. doi: 10.1039/c5nr00893j
- Reviakine, L., Johannsmann, D., and Richter, R. P. (2011). Hearing what you cannot see and visualizing what you hear: interpreting quartz crystal microbalance data from solvated interfaces. *Anal. Chem.* 83, 8838–8848. doi: 10.1021/ac201778h
- Singhal, C., Khanuja, M., Chaudhary, N., Pundir, C. S., and Narang, J. (2018). Detection of chikungunya virus DNA using two-dimensional MoS₂ nanosheets based disposable biosensor. *Sci. Rep.* 8:7734. doi: 10.1038/s41598-018-25824-8
- Song, C. Q., Yang, C. Y., Wang, F., Ding, D. D., Gao, Y., Guo, W., et al. (2017). MoS₂-Based multipurpose theranostic nanoplatform: realizing dual-imaging-guided combination phototherapy to eliminate solid tumor via a liquefaction necrosis process. *J. Mater. Chem. B* 5, 9015–9024. doi: 10.1039/c7tb02648j
- Song, H., Ni, Y. N., and Kokot, S. (2014). Investigations of an electrochemical platform based on the layered MoS₂-graphene and horseradish peroxidase nanocomposite for direct electrochemistry and electrocatalysis. *Biosens. Bioelectron.* 56, 137–143. doi: 10.1016/j.bios.2014.01.014
- Sun, B., Zhang, Y. Q., Chen, W., Wang, K. K., and Zhu, L. Y. (2018). Concentration dependent effects of bovine serum albumin on graphene oxide colloidal stability in aquatic environment. *Environ. Sci. Technol.* 52, 7212–7219. doi: 10.1021/acs.est.7b06218
- Tan, C., and Zhang, H. (2015). Two-dimensional transition metal dichalcogenide nanosheet-based composites. *Chem. Soc. Rev.* 44, 2713–2731. doi: 10.1039/c4cs00182f
- Wang, L. S., Boulaire, J., Chan, P. P. Y., Chung, J. E., and Kurisawa, M. (2010). The role of stiffness of gelatin-hydroxyphenylpropionic acid hydrogels formed by enzyme-mediated crosslinking on the differentiation of human mesenchymal stem cell. *Biomaterials* 31, 8608–8616. doi: 10.1016/j.biomaterials.2010.07.075
- Wang, Y., Wang, X., Wang, J., Zhao, Y. M., He, W. J., and Guo, Z. J. (2011). Noncovalent interactions between a trinuclear monofunctional platinum complex and human serum albumin. *Inorg. Chem.* 50, 12661–12668. doi: 10.1021/ic201712e
- Wani, T. A., Bakheit, A. H., Abounassif, M. A., and Zargar, S. (2018). Study of interactions of an anticancer drug neratinib with bovine serum albumin: spectroscopic and molecular docking approach. *Front. Chem.* 6:47. doi: 10.3389/fchem.2018.00047
- Xia, T., Fortner, J. D., Zhu, D. Q., Qi, Z. C., and Chen, W. (2015). Transport of sulfide-reduced graphene oxide in saturated quartz sand: cation-dependent retention mechanisms. *Environ. Sci. Technol.* 49, 11468–11475. doi: 10.1021/acs.est.5b02349

- Xiao, M., Wei, S., Li, Y. X., Jasensky, J., Chen, J. J., Brooks, C. L., et al. (2018). Molecular interactions between single layered MoS₂ and biological molecules. *Chem. Sci.* 9, 1769–1773. doi: 10.1039/c7sc04884j
- Yin, W., Yan, L., Yu, J., Tian, G., Zhou, L. J., Zheng, X. P., et al. (2014). High-throughput synthesis of single-layer MoS₂ nanosheets as a near-infrared photothermal-triggered drug delivery for effective cancer therapy. *ACS Nano* 8, 6922–6933. doi: 10.1021/nn501647j
- Yousefi, N., and Tufenkji, N. (2016). Probing the interaction between nanoparticles and lipid membranes by quartz crystal microbalance with dissipation monitoring. *Front. Chem.* 4:46. doi: 10.3389/fchem.2016.00046
- Yu, Y. D., Wu, N., Li, Y. L., Li, Y. Y., Zhang, L., Yang, Q., et al. (2017). Dispersible MoS₂ nanosheets activated TGF-beta/Smad pathway and perturbed the metabolome of human dermal fibroblasts. *ACS Biomater. Sci. Eng.* 3, 3261–3272. doi: 10.1021/acsbomaterials.7b00575
- Zamolo, V. A., Modugno, G., Lubian, E., Cazzolaro, A., Mancin, F., Giotta, L., et al. (2018). Selective targeting of proteins by hybrid polyoxometalates: interaction between a Bis-biotinylated hybrid conjugate and avidin. *Front. Chem.* 6:278. doi: 10.3389/fchem.2018.00278
- Zhang, X., Lai, Z. C., Ma, Q. L., and Zhang, H. (2018). Novel structured transition metal dichalcogenide nanosheets. *Chem. Soc. Rev.* 47, 3301–3338. doi: 10.1039/c8cs00094h

Conflict of Interest Statement: The authors declare that the research was conducted in the absence of any commercial or financial relationships that could be construed as a potential conflict of interest.

Copyright © 2019 Liu, Yu, Huang, Su, Qi and He. This is an open-access article distributed under the terms of the Creative Commons Attribution License (CC BY). The use, distribution or reproduction in other forums is permitted, provided the original author(s) and the copyright owner(s) are credited and that the original publication in this journal is cited, in accordance with accepted academic practice. No use, distribution or reproduction is permitted which does not comply with these terms.